



Impact of redox cycles on Mn, Fe, Co and Pb in nodules

S. Cornu^{a*}, J.A. Cattle^{a,b}, A. Samouëlian^a, C. Laveuf^a, L.R.G. Guilherme^{a,c,d}, P. Albéric^e

- a- INRA, UR0272 Science du sol, F-45166 Olivet
- b- Ecotoxicology and Environmental Contaminants Section, Dept of Environment and Climate Change, NSW. PO Box A290, Sydney South, NSW 1232, Australia
- c- le STUDIUM Institute for Advanced Studies, 3D avenue de la Recherche scientifique, 45071 Orléans CEDEX 2, France
- d- Federal University of Lavras, Soil Science Dept., CP 3037, 37200-000 Lavras (MG), Brazil; CNPq (Brazilian Ministry of Science and Technology) Scholar
- e- ISTO UMR 6113 - CNRS/Université d'Orléans, 1A, rue de la Férollerie, 45071 Orléans CEDEX 2, France

Corresponding author: Sophie Cornu

INRA, UR1119 Géochimie des Sols et des Eaux, Europôle de l'Arbois, BP 80, F-13545 Aix en Provence cedex 4.

Sophie.Cornu@aix.inra.fr

Acknowledgments

The authors would particularly like to thank O. Josière, B. Renaux, P. Courtemanche, A. Besnault and C. Le Lay for technical support. This study was funded by the Conseil Régional of Région Centre through the METALOE project and benefited from a STUDIUM fellowship. J.Cattle is grateful to INRA, Orleans, for providing funding for this project.

Impact of redox cycles on Mn, Fe, Co and Pb in nodules

Abstract

Redox processes are responsible for iron and manganese segregation as Fe-Mn oxide coatings or nodules. These nodules are also trace element scavengers in soils. Redox processes are of particular importance in seasonally saturated soil containing naturally high concentrations of trace metals. Here we report the dynamics of Fe-Mn nodules and two associated trace elements, Co and Pb, studied under controlled redox conditions in a column experiment, including 5 columns fed with mimicked topsoil solution. The obtained water was rich in Fe and Mn. This water was then percolating the nodule columns. The results show that the redox conditions reached 100 mV, which was sufficient to dissolve Mn oxides and release the associated Co, while Pb was readsorbed onto nodule surfaces. The amounts of Mn and Co released into the water were small compared to the quantities stored in the nodules (less than 1 ‰ of the initial stock stored in the nodules). The redox conditions were however insufficient to allow Fe oxide dissolution. On the contrary, 70 of 90% of the Fe entering the column was fixed onto the nodules. The number of drying cycles was too small to draw a firm conclusion on their impact on the nodule fate and metal release. However, in terms of environmental threat, these results showed that Pb would not be released from soil during nodule dissolution, whereas Co, which is less toxic, would be released.

Introduction

Nodules of Mn and Fe oxides are commonly found in different soil types where they have been extensively studied (Childs and Leslie, 1977; Dawson et al., 1985; Latrille et al., 2001; Palumbo et al., 2001; Liu et al., 2002). They are generally made of both Mn and Fe oxide cements, both elements having a different spatial distribution within nodules (Dawson et al., 1985; Palumbo et al., 2001; Liu et al., 2002), surrounding detrital grains of varying nature according to the soil context (Latrille et al., 2001; Palumbo et al., 2001; Liu et al., 2002; Cornu et al., 2005).

Iron oxides of nodules consist in goethite (Fitzpatrick, 1988) and either hematite (Herbillon and Nahon, 1988) or ferrihydrite (Cornu et al., 2005) according to the soil type. Hematite is mostly found in nodules formed in tropical soils while ferrihydrite is found in those formed under temperate conditions. Manganese oxides in nodules consist mainly of birnessite and lithiophorite (Taylor, 1968; Manceau et al., 2002; 2003; Neaman et al., 2004).

Nodules are well-known for their high content in trace elements. Cobalt, Ni, and Zn are frequently associated with the Mn-rich parts of nodules (Childs and Leslie, 1977; Dawson et al., 1985; Latrille et al., 2001; Liu et al., 2002; Manceau et al. 2002; Neaman et al., 2004, 2008), while Cr (Liu et al. 2002) and Pb (Latrille et al. 2001; Palumbo et al., 2001; Neaman et al., 2004, 2008) are associated with Fe-rich parts. McKenzie (1975), Childs and Leslie (1977), Dawson et al. (1985), Latrille et al. (2001), Palumbo et al. (2001) and Liu et al. (2002) showed that Cu and Mn partitioning between Fe and Mn oxides in nodules is variable. In some soils, nodules can even be the main trace element scavenger (Cornu et al., 2005).

These nodules are formed in horizons undergoing past or present seasonal waterlogging (McKenzie, 1989 and references herein; Khan and Fenton, 1994; Zhang and Karathanasis, 1997). In environments still undergoing seasonal waterlogging, nodules are sensitive to variation in pH and Eh, and can be both source and sink of trace elements

according to the intensity, and possibly also the duration, of the reduction phase (Jenne, 1968; Zaidel'man and Nikiforova, 1998; Cambier and Charlatchaka, 1999). This process is of prime importance in wetlands undergoing seasonal waterlogging periods that can last for several months (D'Amore et al., 2004). Grybos et al. (2007) demonstrated that the fate of Fe-Mn oxides in wetlands was entirely responsible for the fate of Co and partially for that of Pb and Ni, while the impact of redox conditions on Cu and Cr was less clear.

Climate change has affected the duration of the annual waterlogging period, such that it is either reduced or increased according to the latitude (IPCC, 2001). An understanding of the dynamics and the fate of Fe and Mn in nodules, as well as their associated trace elements is of importance in predicting their environmental impact in ecosystems such as wetlands.

Several studies report the impact of redox cycles on the fate of Fe oxides (Thompson et al., 2006), and Fe and Mn oxides and their associated trace elements (Quantin et al., 2001; 2002; Feder et al., 2005; Contin et al., 2007; Grybos et al., 2007). However, these oxides were dispersed into the soil matrix and, to our knowledge, no attempt was made to understand the sorption and release of trace elements from soil nodules that are the main trace element scavengers in soils (Cornu et al., 2005) and have different accessibility to soil solution than the dispersed oxides.

We aim here to investigate the effect of redox cycles on the mobility of Fe and Mn in soil nodules and of the associated Co and Pb coming from temperate climate. For that an original experimental design using nodule column experiments was designed in order to mimic natural conditions of redox cycles that occur in subsurface soil horizons.

Material and Methods

Site and soil

The study site, located on the Aigurande plateau in the Massif Central, is underlain by amphibolite and gneiss. On the footslope, Planosols (FAO, 2006) – or Albaqualfs (Soil Taxonomy, 1999) – developed on gneiss (Salvador-Blanes, 2002). The upper horizons of the Planosols are allochthonous and derived from silty, colluvial materials of amphibolitic and gneissic origin, while the deeper clayey B horizon (below 50 cm depth) and the alterite are developed in gneiss. Colluvial materials differentiate into three horizons: a sandy-loam to clay-loam organic-rich A horizon (25 to 30 cm thick) and two E horizons, one of them being rich in Fe/Mn-nodules and gravels (Cornu et al., 2005). The nodule-rich horizon is a sink for Fe, Mn, Co and Pb (Table 1; Cornu et al., 2005). Cornu et al. (2005) showed that Mn oxides preferentially scavenge Co and Pb. The E horizons are waterlogged during winter and spring due to the texture contrast with the underlying B horizon. The duration of the waterlogging period increases down the slope. This horizon is draining most of the water of a 6-ha plot.

Soil water quality was monitored on this site by Penfrêne (2008). From the data they provided (Penfrêne, 2008 and references herein), we estimated that the average effective rainfall for the region ranges from 200 to 300 mm.

The nodule rich E horizon and the associated top horizon were sampled from a midslope position equivalent to that of pit 2 in Cornu et al. (2005).

Column preparation and characterisation

Nodules were sorted from the rest of the soil and carefully cleaned. They were then separated from the bulk soil matrix by wet sieving. For practical reasons, only the 2-5 mm fraction was collected and oven dried at 40°C. Nodules were manually sorted with tweezers until ~500 mL of nodules were obtained. To remove nodule clay coatings, nodules were then

placed into 250-mL screw cap bottles containing ultrapure water (nodules:water 1:1 v/v). The bottles were placed on an end-over-end shaker and rotated at 100 rpm for eight hours. Water was changed after ~ four hours by tipping nodules onto a 1-mm sieve, followed by discarding and rinsing excess clay suspension through the sieve with ultrapure water. Nodules were then washed (as above) on the sieve and left covered in a tray overnight. This process was repeated for seven days. Nodules were then sieved into 3-4 mm and 4-5 mm fractions (nodules <3mm comprised only 1.5% of the total and were not used). Each column contained equivalent amounts of each fraction. To keep the natural soil nodule particle-size distribution, 34.2 g of 3-4 mm nodules and 43.5 g of 4-5 mm nodules were weighed into each column (Table 2). We thus ensured that all the columns had the same characteristics in terms of chemistry, pore volume and surface area. A subset of nodules not used in the column experiment was kept aside for determination of BET (Brunauer, Emmett and Teller) surface area measurement, total elemental analysis by ICP-AES after triacid HF dissolution, and solid density with a pycnometer (Table 1).

Quartz sand (purchased commercially) was used as a control. It was sieved to be in the size fraction 0.4-1 mm. This size fraction was used to favour the formation of nodules around sand particles (this sand also contained small amounts of micas and feldspars as shown by X-ray diffraction; results not shown). Quartz sand was packed into the column on a volume basis matching that of the nodule columns, i.e. ~98 g (Table 2). A sub-sample was kept for characterisations as described for the nodules (Table 1).

Experimental setting

The experimental design is shown schematically in Figure 1. This consists in two main parts: part A designed to produce a water whose quality mimicked that of a natural one and part B that consists in the column experiment itself.

The percolating water was produced by passing ultrapure water through a topsoil monolith. A topsoil monolith of 20x13x16 cm in size was sampled from the surface A horizon directly above the sampled nodule-rich E horizon. This monolith was removed from the ground in a plastic box. The plastic box had four inlets in the surface, one outlet at the top of one side (used as a drain when necessary) and two outlets at the base on the opposite side. One of these outlets was used as the source of water to pass through the columns and the other worked as a port for sampling the inflowing column water for separate measurements. The so-produced inflow water was sampled and analysed for each sampling date (see below).

At the start of the experiment the surface horizon monolith had a moisture content of 37% (field moisture content). Prior to the experiment it was saturated from the base over a period of four hours. A total of 1700 mL of ultrapure water was required to saturate the block. Saturation continued until free water ponded on the soil surface, when the box was then connected to the columns.

Water percolated through the topsoil monolith was then pumped (via a peristaltic pump) through each of five columns. Columns were fashioned from standard syringes (60 mL) with Teflon[®] tubing as inlet and outlet and were wrapped in Al-foil to avoid photo-oxidation. A layer of nylon mesh was placed at the base of each column to prevent fine material blocking the column outlet. A silicon stopper was used in each column to form a seal. A number of multi-feeder taps (5 taps from a single inlet; see Figure 1) linked all columns to the pump to ensure an equivalent inflow rate for each treatment. All equipment was acid-washed and blanks were performed by pumping ultrapure water through the empty system (blank readings were all below the detection limit of the analytical procedures described thereafter).

The experiment was conducted in a glove box under an oxygen-depleted atmosphere (using N₂), with treatments as follows:

(i) nodules (in duplicate) and quartz continuously saturated for 6 months;

(ii) nodules and quartz subjected to 14-day wetting and drying cycles. Columns undergoing drying cycles were removed from the glove box to enable exposure to oxygen.

Water sampling and analysis

Column leachates were collected daily over the first month of the experiment and three times a week for the rest of the experiment, which lasted over six months. Electrical conductivity (EC), pH, and redox potential (Eh) were measured immediately on sample collection in the glove box. Redox potential was measured using an Ag/AgCl electrode and Eh measurements were then corrected to the standard hydrogen electrode, by using a correction factor depending on the temperature (Kölling, 1999).

$$Eh_{\text{corrected}} = Eh_{\text{measured}} + (207 + 0.7 (25-T))$$

where T is the temperature in °C, and $Eh_{\text{corrected}}$ is the corrected redox potential in mV. Experiments were performed at room temperature (~25°C).

As only Eh corrected values are presented in the rest of the paper they are referred as Eh for simplicity.

After collection, samples were removed from the glove box for immediate filtering (< 0.2 µm on cellulose acetate membrane). A part of the sample was then kept aside while the rest was acidified with suprapur HNO₃ for subsequent analysis by atomic absorption spectroscopy using flame for Fe and Mn, and graphite furnace for Co and Pb.

Eh-pH diagrams

Data were reported in Eh - pH stability diagrams (Brookins, 1988; McBride, 1994) for Mn and Fe species. For the manganese diagram, as no clear identification of the Mn oxide present into the nodule was available (Cornu et al., 2005), the most common Mn oxides found in

nodules were taken into account: birnessite ($\text{Mn}_5^{4+} \text{Mn}_2^{3+} \text{O}_{13}$) and lithiophorite ($\text{Al}_2\text{Mn}_3^{4+} \text{O}_9$) (Taylor, 1968; Manceau et al., 2002; 2003; Neaman et al., 2004). For iron diagrams, either ferrihydrite ($\text{Fe}_2\text{O}_3 \cdot 0.5(\text{H}_2\text{O})$) or goethite (FeOOH) with two possibilities γ or α forms were considered as these two last minerals are observed in the nodules by Cornu et al. (2005). Green rusts were also considered in the form ($\text{Fe}(\text{OH})_3$) and ($\text{Fe}_3(\text{OH})_8$) even if not identified as these minerals are transitory (Trolard and Bourrié, 1999; Feder et al., 2005). Thermodynamic constants related to the different solids phases are reported in Table 3. Data from column outflows were plotted on Eh-pH diagrams in order to estimate the potential equilibrium or disequilibrium with minerals present in the nodules when redox conditions reached 100 mV.

Statistic treatment

In order to determine if the discrepancies observed between the different columns were statistically significant, ANOVA tests were performed. This test was applied to the data obtained once the reduced conditions were reached. For each column, measurements were then considered as different repetitions. One ANOVA analysis was performed for each of the studied variable: pH, Eh, Fe, Mn, Co, and Pb. The results were combined in Tables 4 and 5.

Results and discussion

Characteristics of the water inflow along the experiment: quality and quantity

The solution percolating through the soil monolith (column inflow) had an initial pH fluctuating from 6.6 to 6.95, increasing slightly over time to a more stable pH range of 6.85 to 6.95 (Fig. 2a; average pH value of 6.75). The pH values were of the same order of magnitude as those recorded in the field by Pelfrêne (2008), for the same site.

Redox potential decreased from values higher than 360 mV at the beginning of the experiment to values fluctuating between 90 and 120 mV after 30 days (Fig. 2b). Eh values stayed in this range (moderately reducing conditions) until the end of the experiment. The lag time needed for the re-establishment of reducing conditions in different laboratory experiments is reported to range from 100 hours (Grybos et al., 2007) to 20 days (Quantin et al., 2001). In the field, D'Amore et al. (2004) reported that this time ranged from a few days to three months according to the depth and the amount of rain. Our results (30 days) are in agreement with these data. In addition, these Eh values are of the same order of magnitude as those recorded in the field by D'Amore et al. (2004) for wetlands, although these authors did record more reducing conditions during the wettest years. This range of Eh was also reached by Quantin et al. (2001) and Thompson et al. (2006) in their experiments, while the experiments of Grybos et al. (2007) reached lower redox potentials. Their Eh values were lower than the minimum value recorded in the field by D'Amore et al. (2004). Unfortunately, no Eh values were recorded by Pelfrêne (2008) for this site. Quantin et al. (2001) showed that an Eh decrease occurred only in biologically active samples and interpreted it as the result of biological activity.

Iron concentrations were about $\sim 0.018 \text{ mmol L}^{-1}$ over the 10 first days of the experiment, rising to $\sim 0.18 \text{ mmol L}^{-1}$ after 20 days and to 0.36 mmol L^{-1} after 35 days (Fig.

2c). Concentrations oscillated around this value for the duration of the experiment. Thompson et al. (2006) and Quantin et al. (2001) observed Fe oxide dissolution with comparable Eh values. Eh-pH diagrams for Fe (Fig. 3a) show that solutions coming out of the soil monolith are oversaturated with respect to all Fe-oxides present in the nodules.

Manganese concentrations increased rapidly at the beginning of the experiment, reaching a value of 0.27 mmol L^{-1} after 20 days (Fig. 2d). Manganese concentrations in the soil leachates (column inflow) were of the same order of magnitude as those recorded for Fe. The inflow data (Table 4) revealed dissolution of Fe and Mn oxides at a molar Mn/Fe ratio of 0.61, whereas the surface horizon had a solid phase molar Mn/Fe ratio of 0.03 (ratio calculated from data in Table 1). This means that Mn oxides were proportionately more dissolved – about 20 folds – than Fe oxides, which is consistent with the higher sensitivity of Mn oxides to redox conditions compared with Fe oxides (Jenne, 1968; Stumm and Morgan, 1981) and also with data reported by Quantin et al. (2001). After 20 days, Mn concentrations gradually decreased to reach a value of 0.09 mmol L^{-1} at the end of the experiment. The Eh-pH diagram for Mn (Fig. 4) shows that solutions coming out of the soil monolith are undersaturated with respect to both birnessite and lithiophorite. The dissolution of these two minerals is thus probably responsible for the Mn concentrations acquired by the percolating waters.

Trends observed for cobalt paralleled those described for Mn (Fig. 2e). With the exception of two high concentrations, lead concentrations decreased sharply from $0.019 \text{ } \mu\text{mol L}^{-1}$ to about $0.005 \text{ } \mu\text{mol L}^{-1}$ at 40 days and stabilised thereafter (Fig. 2f).

The obtained reducing conditions were sufficient to dissolve both iron and manganese oxides from the topsoil monolith, also observed in the experiments of Quantin et al (2001) and Thompson et al. (2006). Patrick and Jugsujinga (1992) give lower Eh values for the

reduction of Fe oxides (50 mV), while their data for Mn oxides are in agreement with results reported here.

After 80 days of the experiment the data became very noisy. The monolith structure started to collapse and had to be replaced. This change produced sample oxidation, and reducing conditions were not observed again before the end of the experiment (data not shown). For this reason only data obtained for the 80 first days of the experiment are presented here.

Impact of the redox condition on the release of Fe, Mn and associated trace elements by nodules

As shown in Table 6, the amount of water percolated through the different columns was reasonably similar despite the difficulties in regulating the water flow. The difference between the continuously saturated treatment and the 14-day wetting and drying cycle treatment was due to no solution leaching during the drying cycle. Given that the quartz and nodule columns had such different pore volumes (Table 2), percolated volumes have been expressed in terms of pore volumes hereafter to allow comparison.

Outflow from the columns had a significantly higher pH (around 7.1 overall; Figs. 5a to 8a) than the inflow according to an ANOVA test at a 5% confidence level (Table 4).

The outflow Eh followed the same general trend as the inflow, decreasing sharply over the first month and then stabilising (Figs. 5b to 8b). Once stabilised, the outflow Eh from the quartz column before the drying cycle was not significantly different from that of the inflow, according to an ANOVA test at a 5% confidence level (Table 4). Nodule columns had a significantly higher Eh in the outflow (ANOVA test at a 5% confidence level, Table 4), especially those undergoing drying cycles.

Iron concentrations in both column inflow and outflow increased initially, reaching a relatively stable level at about 35 days (Figs. 5c to 8c). Subsequent Fe concentrations in the outflow were significantly lower than those of the inflow (ANOVA test at a 5% confidence level, Table 4) suggesting Fe fixation within the columns. The outflow from quartz columns contained higher Fe concentrations than that from the nodule columns (ANOVA test at a 5% confidence level, Table 4). The nodule column undergoing wetting and drying cycles had the smallest outflow Fe concentrations, which could be related to the higher Eh values also recorded for this column. As inflow Fe concentrations slightly changed over time, fixation ratios were calculated to compare the fixation of Fe between the different columns as follows:

$$Fe_{\text{fixation ratio}} = ([Fe]_{\text{in}} - [Fe]_{\text{out}}) / [Fe]_{\text{in}}$$

An ANOVA test at a 5% confidence level showed that the fixation ratio of the quartz column undergoing wetting and drying cycles was the lowest before drying and the nodule column undergoing wetting and drying cycles fixed more Fe than the other nodule columns (Table 5). Thus nodule columns were able to fix Fe more efficiently than quartz columns. Eh-pH diagrams for Fe (Fig. 3) show that column outflows are oversaturated with respect to goethite, ferrihydrite and one green rust type ($Fe(OH)_3$). The Fe fraction retained in the columns was thus probably precipitate as goethite, ferrihydrite and one green rust type along the experiment. Green rust, which is a transitory phase, was probably then recrystallised into goethite or ferrihydrite as 40% and 25% of the Fe contained in the nodules was into these minerals respectively (Cornu et al., 2005).

Similarly to Fe, outflow Mn concentrations increased following the increase in inflow concentrations (Figs. 5d to 8d). Once stabilised, Mn concentrations in column outflows were significantly higher than column inflows (ANOVA test at a 5% confidence level, Table 4). Manganese concentrations in outflows of nodule columns were also higher than those of quartz columns, indicating a release of Mn from nodules into the water. We have expressed

the Mn released from the column in terms of a release ratio to better compare the different treatments:

$$\text{Mn}_{\text{release ratio}} = ([\text{Mn}]_{\text{out}} - [\text{Mn}]_{\text{in}}) / [\text{Mn}]_{\text{in}}$$

An ANOVA test at a 5% confidence level confirmed these results (Table 5). The Eh-pH diagram for Mn shows that nearly all column outflows are undersaturated with respect to birnessite and lithiophorite (Fig. 4). As manganese oxides contained 100% of the Mn present in the nodules (Cornu et al., 2005), the dissolution of these minerals is responsible for the increase in Mn concentrations in outflows from the nodule columns.

Results show that while Fe was fixed within the columns during the experiment, reduction processes released Mn. Thus, the reducing conditions were strong enough to dissolve Mn oxide but not sufficient to dissolve Fe oxides.

Cobalt concentrations in column outflows increased with those in the inflow and stabilised after 35 days (Figs. 5e to 8e). Once stabilised, inflow and outflow Co concentrations in quartz columns were not significantly different (ANOVA test at a 5% confidence level, Table 4). Outflow Co concentrations from nodule columns were significantly higher than inflow concentrations indicating a net release of Co from nodules. As for Mn we calculated a Co release ratio. The results for the Co release ratio were equivalent to those from Co concentrations (ANOVA test at a 5% confidence level, Table 5). As for Mn, 100% of the Co found in the nodules was contained in Mn oxides (Cornu et al., 2005). The Co/Mn ratios of the Mn and Co released from the nodule columns were close to those of the nodules, suggesting that dissolution of Mn oxide evidenced previously is responsible for Co losses. It also suggests that readsorption does not occur within the column unless it is in the same proportion for the two elements as that originally present in the solid phases, which disagrees with results of Quantin et al. (2002) who showed that Co

concentrations decreased over time. This was interpreted as readsorption. Such behaviour was not exhibited in our experiment.

As observed for the inflow, outflow Pb concentrations decreased sharply over time and stabilised at low values with the exception of some discrepancies (Figs. 5f to 8f). If we exclude these few very high concentrations, outflow Pb concentrations from columns undergoing wetting and drying cycles were significantly higher than those of the inflow, while those of the permanently saturated column were significantly lower (ANOVA test at a 5% confidence level, Table 4). While there was no obvious explanation for this behaviour, the overall concentrations were very low. When the ANOVA was performed with the high concentrations included no significant differences were found (ANOVA test at a 5% confidence level; results not shown). Cornu et al. (2005) showed that Pb was present at almost 90% in Mn nodules; however, no Pb was either added to or removed from the water suggesting that either the Mn oxides were not dissolved congruently or that the Pb was re-adsorbed on the remaining phases in the column. Indeed, McKenzie (1989 and references herein) stated that in general Mn oxides adsorbed more Pb than Co. The same was recorded for Fe-oxides (Schwertmann and Taylor, 1989 and references herein).

Impact of the drying on the following reducing period

The drying cycle caused a slight increase in the outflow pH from the nodule column (Fig. 8a) although this difference was not significant according to an ANOVA test (Table 4). For the quartz column, the effect of the drying cycles was even smaller (Fig. 7a).

Outflow Eh values increased significantly after the drying period in the quartz column (ANOVA test at a 5% confidence level, Table 4), becoming equivalent to outflow Eh values recorded for nodule columns always saturated (Table 4). This increase of Eh upon drying was

less clear for the nodule column, which already exhibited a higher outflow Eh before drying than the continuously saturated nodule columns.

Iron concentrations in outflows from the quartz column dropped significantly after drying (ANOVA test at a 5% confidence level, Table 4), however the concentrations increased quickly again (Fig. 7c). Only a slight decrease (not significant) was observed in the nodule column, possibly due to its low original Fe concentrations. The fixation ratios, show that both quartz and nodule columns fixed significantly more Fe after drying (ANOVA test at a 5% confidence level, Table 5). For these two columns, the Fe fixation ratio was closely related to Eh values of the column outflow (Fig. 9). The drying cycle clearly increased the efficiency of the nodules to fix Fe. Contin et al. (2007) also reported an increase in trace metal retention upon reoxidation of oxides following consecutive redox cycles. Eh-pH diagrams for Fe (Fig. 3b) show that after a drying period, column outflows are also oversaturated with respect to $\text{Fe}_3(\text{OH})_8$, which was rarely the case before the drying. Thus, more Fe oxide types are potentially responsible for the Fe uptake from the solution by the column.

The drying cycles caused outflow Mn concentrations to drop significantly (ANOVA test at a 5% confidence level, Table 4). For the quartz column, the concentrations became even lower than those of the inflow, indicating Mn fixation. For the nodule column, outflow Mn concentrations remained higher than those of the inflow, revealing Mn release. When considered in terms of the Mn release ratio, the impact of the drying cycle was smaller in nodule columns than in quartz columns (Table 5). The Eh-pH diagram for Mn (Fig. 4) did not evidence a clear difference in terms of solution equilibrium with respect to birnessite and lithiophorite before and after drying. Both type of solutions were mainly understaturated with respect to these minerals.

The drying period provoked a net decrease in the outflow Co concentrations from the quartz column, which were significantly lower than the inflow concentrations (ANOVA test

at a 5% confidence level, Table 4). This fixation of Co within the quartz column (as was seen for Mn) is small and not significant when expressed in terms of ratio (ANOVA test at a 5% confidence level, Table 5). Surprisingly, outflow Co concentrations from the nodule column increased significantly after drying, which could be better seen when expressed in terms of release ratio (ANOVA test at a 5% confidence level, Table 5).

The drying period increased the Eh within nodule columns, inducing a larger Fe fixation. The influence of these cycles on other elements was less clear. A slightly lower Mn release was recorded. Cobalt release was however found to be larger; this result was not consistent with a decrease in Mn release and Co being contained within Mn oxides. All these trends were unable to be clearly interpreted and more wetting and drying cycles should be performed in order to draw a firm conclusion.

Consequences of the redox cycles in terms of soil evolution and environmental impact

The total gains in Fe and respective losses in Mn and Co were calculated by mass balance calculation on the inflow and outflow waters and reported in Table 7. They are several orders of magnitude lower than the stocks of these elements found in the different columns (Table 2) and are thus negligible compared with the amount of these elements initially present in the nodules. This was confirmed by analyses of the solid phase at the end of the experiment, which showed no difference from analyses performed on nodules and quartz sand before the experiment (results not shown). We do not expect much of a change in the forms of Fe and Mn present in nodules, owing to the small magnitude of the gains or losses that occurred throughout the experiment. For this reason we did not perform any sequential extractions after the experiment as was done in some other studies reporting much larger releases of Fe and/or Mn (Quantin et al., 2002; Thompson et al., 2006). In these studies

the focus was on the fine earth soil fraction. Our results demonstrate that in the case of nodules the rate of release of these elements as a function of redox processes is slow.

Reducing conditions lead to a slow increase in Fe content and dissolution of Mn oxides, which released associated Co. Lead (also contained in Mn oxides of the nodules) was not lost, as it was probably readsorbed on the remaining phases. Despite the over-saturation of the percolating solutions with respect to green rusts, the only Fe oxides identified in these nodules were goethite and ferrihydrite (Cornu et al., 2005).

We can conclude that the nodules in the studied soils are still active but that their reactivity is very low, as shown by the low amount of Fe and Mn fixed or released with an amount of percolated water that was equivalent to 8 m. However, this study showed that nodules were very efficient Fe scavengers as they fixed 70 to 90% of the Fe initially present in the water (Table 5).

The water running out of the column experiment has concentrations ranging from 0.01 to 0.39 mmol L⁻¹ for Fe, from 0 to 0.43 mmol L⁻¹ for Mn, from 0.01 to 1.43 μmol L⁻¹ for Co and from 10⁻⁴ to 0.07 μmol L⁻¹ for Pb. This water directly runs out in a small river. However, the concentrations in Pb are very low as they never exceed the acceptable limit for drinking water of 0.048 μmol L⁻¹. This is also the case for Co concentrations, which are lower than the limit concentration for waste water release into the environment. However, Fe and Mn concentrations are generally higher, from one to several orders of magnitude, than the limit given by the European Directive – of June, 16th 1975 – for surface waters. Thus the only potential threat to the surrounding water will come from Fe and Mn and not from the trace elements. However, as Mn is very sensitive to change in redox conditions, it will precipitate easily and probably shall not reach the river. Indeed Pelfrêne (2008) gives Fe concentrations in water for this horizon that are on the same order of magnitude as the ones obtained in this study, while their Mn concentrations are one order of magnitude lower. At last, only Fe may

represent a threat for the environment, as it is the only one exceeding in the soil water the limit concentration given by the European Directive of June, 16th 1976.

Conclusion

Simulating redox cycles in a laboratory experiment on soil nodules showed that redox conditions similar to those found in soils could be achieved. These conditions allow reduction of Mn oxides, while Fe oxides were still precipitated. Both the experiment and the Eh-pH diagram results were consistent with these findings. The process was relatively slow as only a very small fraction of the Mn and Fe contained in the nodules was either released or fixed. This suggested that if still active, the process of formation/dissolution of nodules in soils is slow.

These nodules are a sink for trace elements. In this study we showed that while Co was released at the same rate as Mn, Pb also contained in Mn oxides was not released from the column and was probably re-adsorbed on nodule surfaces. This suggested that the knowledge of the trace element location as determined by sequential extraction is not sufficient to determine the fate of a trace element in the environment. Such extractions must be combined with other types of experiment.

Finally, redox cycles including a drying period would reduce the release of Co, given that Mn oxide formation would occur with concurrent adsorption of Co. Due to technical difficulties in conducting this experiment, only one complete redox cycle could be achieved. More redox cycles of different duration should be performed in order to be able to predict the impact of waterlogging duration on nodule fate either through agricultural practices (irrigation/drainage) or due to climate change.

In terms of environmental threat this result also suggests that Pb would not be released from soil during nodule dissolution, whereas Co, which is less toxic, would be released.

References

- Brookins, D.G. 1988. Eh-pH diagrams for geochemistry. Springer-Verlag, New York, 176 p.
- Cambier, P. and Charlatchaka, R. 1999. Influence of reducing conditions on the mobility of divalent trace metals in soils. In: H.M. Selim and I.K. Iskandar (Eds.). Fate and transport of heavy metals in the vadose zone. Lewis Publishers, Boca Raton, p. 159-175.
- Childs, C.W. and Leslie, D.M. 1977. Interelement relationships in iron-manganese concretions from a catenary sequence of yellow-grey earth soils in loess. *Soil Science*, 123(6): 369-376.
- Contin, M., Mondini, C., Leita, L. and De Nobili, M. 2007. Enhanced soil toxic metal fixation in iron (hydr)oxides by redox cycles. *Geoderma*, 140:164-175.
- Cornu S., Deschatrettes V., Salvador-Blanes S., Clozel B., Hardy M., Branchut S., Le Forestier L. 2005, Trace element accumulation in Mn-Fe-oxide nodules of a planosolic horizon. *Geoderma*, 125:11-24.
- D'Amore, D.V., Stewart, S.R. and Huddleston, J.H. 2004. Saturation, reduction and formation of iron-manganese concretions in the Jackson-Frazier Wetland, Oregon. *Soil Sci. Soc. Am. J.*, 68:1012-1022.
- Dawson, B.S.W., Fergusson, J.E., Campbell, A.S. and Cutler, E.J.B. 1985. Distribution of elements in some Fe-Mn nodules and an iron-pan in some gley soils of New Zealand. *Geoderma*, 35:127-143.
- Détournay, J., De Miranda, L., Dérié, R. and Ghodsi, M. 1975. The region of stability of green rust II in the electrochemical E-pH equilibrium diagram of iron in sulphate medium. *Corrosion Science*, 15:295-306.
- FAO, 2006. World reference base for soil resources. A framework for international classification, correlation and communication, 128 p.

Feder, F., Trolard, F., Klingelhofer, G. and Bourrié, G. 2005. In situ Mossbauer spectroscopy: Evidence for green rust (fougerite) in a gleysol and its mineralogical transformations with time and depth. *Geochim. Cosmochim. Acta*, 69:4463-4483.

Fitzpatrick, R.W. 1988. Iron compounds as indicators of pedogenic processes: example from southern hemisphere. Chapter 13. In: J.W. Stucki, B.A. Goodman and U. Schwertmann (Eds.). *Iron in soils and clay minerals*. NATO ASI Series, serie C, vol 217, p. 351-396.

Grybos, M., Davranche, M., Gruau, G. and Petitjean, P. 2007. Is trace metal release in wetland soils controlled by organic matter mobility or Fe-oxyhydroxydes reduction? *J. Colloid and Interface Sci.*, 314:490-501.

Hashimoto, K. and Misawa, T. 1973. The solubility of the γFeOOH in perchloric acid at 15°C. *Corrosion Science*, 13:229-231.

Herbillon, A.J. and Nahon, D., 1988. Laterites and lateritization processes. Chapter 22. In: J.W. Stucki, B.A. Goodman and U. Schwertmann (Eds.). *Iron in soils and clay minerals*. NATO ASI Series, serie C, vol 217, p. 779-796.

IPCC. *Climate change 2001: the scientific basis*. Contribution of working group I to the third assessment report of the intergovernmental panel on climate change. Houghton, J. T. et al. (Eds.). Cambridge Univ. Press, Cambridge, 2001.

Jenne, E.A. 1968. Controls on Mn, Fe, Co, Ni, Cu and Zn concentrations in soils and waters: the significant role of hydrous Mn and Fe oxides. In: R.F. Gould (Editor), *Trace inorganics in water*. Adv. Chem. American Chemical Society, p. 337-387.

Khan, F.A. and Fenton, T.E. 1994. Saturated zones and soil morphology in a Mollisol catena of Central Iowa, *Soil Sci. Soc. Am. J.*, 58:1457-1464.

Kölling, M. 1999. Comparison of different methods for redox potential determination in natural waters. In: J. Schüring, H.D. Schulz, W.R. Fisher, J. Bötcher and W.H.M.

Duihnisveld. Redox: Fundamentals, processes and applications. Springer-Verlag, New-York, p. 42-54

Latrille, C., Elsass, F., van Oort, F. and Denaix, L. 2001. Physical speciation of trace metals in Fe-Mn concretions from a rendzic lithosol developed on Sinemurian limestones (France). *Geoderma*, 100:127-146.

Liu, F., Colombo, C., Adamo, P., He, J.Z. and Violante, A. 2002. Trace elements in manganese-iron nodules from a Chinese Alfisol. *Soil Science Soc. Am. J.*, 66:661-670.

Manceau, A., Tamura, N., Marcus, M.A., MacDowell, A.A., Celestre, R.S., Sublett, R.E., Sposito, G. and Padmore, H.A. 2002. Deciphering Ni sequestration in soil ferromanganese nodules by combining X-ray fluorescence, absorption, and diffraction at micrometer scale resolution. *American Mineralogist*, 87:1494-1499.

Manceau, A., Tamura, N., Celestre, R. S., MacDowell, A.A., Geoffroy, N., Sposito, G. and Padmore, H.A. 2003. Molecular-scale speciation of Zn and Ni in soil ferromanganese nodules from loess soils of the Mississippi Basin. *Environ. Sci. Technol.*, 37:75-80.

McBride, M.B. 1994. *Environmental chemistry of soils*. Oxford University Press, Oxford, 406 p.

McKenzie, R.M., 1975. An electron microprobe study of the relationships between heavy metals and manganese and iron in soils and ocean floor nodules. *Australian Journal of Soil Research*, 13:177-188.

McKenzie, R.M. 1989. Manganese oxides and hydroxides. Chapter 9. In: J.B. Dixon and S.B. Weed. (Eds.). *Minerals in soil environments*. SSSA Book Series: 1, Madison, Wisconsin. p. 439-465.

- Neaman, A., Mouele, F., Trolard, F., and Bourrié, G. 2004. Improved methods for selective dissolution of Mn oxides: applications for studying trace element associations. *Applied Geochemistry*, 19:973-979.
- Neaman, A., Martínez, C.E., Trolard, F. and Bourrié, G. 2008. Trace element associations with Fe- and Mn-oxides in soil nodules: Comparison of selective dissolution with electron probe microanalysis. *Applied Geochemistry*, 23:778-782.
- Palumbo, B., Bellanca, A., Neri, R. and Roe, M.J. 2001. Trace metal partitioning in Fe-Mn nodules from Sicilian soils, Italy. *Chemical. Geol.*, 173:257-269.
- Parc, S., Nahon, D., Tardy, Y. and Viellard, P. 1989. Estimated solubility products and fields of stability for cryptomelane, nsutite, birnessite, and lithiophorite based on natural lateritic weathering sequences. *American Mineralogist*, 74:466-475.
- Patrick, W.H. and Jugsujinga, A. 1992. Sequential reduction and oxidation of inorganic nitrogen, manganese and iron in flooded soil. *Soil Sci. Soc. Am. J.*, 56:1071-1073.
- Pelfrêne, A. 2008. Spéciation des métaux traces (Cd, Cu, Pb, Zn) dans les eaux d'un Planosol non pollué (Massif Central, France). Thèse de l'Université François Rabelais de Tours. 190 p.
- Ponnamperuma, F.N., Tianco, E.M. and Loy, T. 1967. Redox equilibria in flooded soils: I. The iron hydroxide systems. *Soil Science*, 103:374-381.
- Quantin, C., Becquer, T., Rouiller, J.H. and Berthelin, J. 2001. Oxide weathering and trace metal release by bacterial reduction in a New Caledonia Ferralsol. *Biogeochem.*, 53:323-340.
- Quantin, C., Becquer, T. and Berthelin, J. 2002. Mn-oxide: a major source of easily mobilisable Co and Ni under reducing conditions in New Caledonia Ferralsols. *C. R. Geoscience*, 334:273-278.

- Rabenhorst and Castenson, 2005. Temperature effects on iron reduction in a hydric soil. *Soil Science*, 170:734-742.
- Salvador-Blanes, S. 2002. Déterminisme de la distribution spatiale des éléments majeurs et traces dans les sols en contexte métamorphique. PhD Thesis, University of Tours, Tours. 283p.
- Schwertmann, U. and Taylor, R.M. 1989. Iron oxides. Chapter 8. In: J.B. Dixon and S.B. Weed. (Eds.). *Minerals in soil environments*. SSSA Book Series: 1, Madison, Wisconsin. p. 379-438.
- Soil Taxonomy. 1999. Basic system of soil classification for making and interpreting soil surveys. United States Department of Agriculture Natural Resources Conservation Service, 871 p.
- Stumm, W. and Morgan, J.J. 1981. *Aquatic Chemistry*. 2 ed. Wiley, New York, 780 p.
- Taylor, R.M. 1968. The association of manganese and cobalt in soils-further observations. *J. Soil Sci.*, 19:77-80.
- Trolard, F. and Bourrié, G. 1999. L'influence des oxydes de fer de type « rouilles vertes » sur les séquences d'oxydo-réduction dans les sols. *Comptes rendus de l'académie des Sciences, Sciences de la Terre et des planètes*, 329:801-806.
- Thompson, A., Chadwick, O.A., Rancourt, D.G. and Chorover, J. 2006. Iron-oxide crystallinity increases during soil redox oscillations. *Geochim. Cosmochim. Acta*, 70:1710-1727.
- Zaidel'man, F.R. and Nikiforova, A.S. 1998. Manganese-iron concretions in soils and their change under the effect of gleyification on parent materials of different genesis. *Eurasian Soil Sci*, 31:817-825.
- Zhang, M. and Karathanasis, A.D. 1997. Characterization of iron-manganese concretions in Kentucky Alfisols with perched water tables. *Clays Clay Miner.*, 45:428-439.

Table 1: Characteristics of the solids used in the experiment[†]

Sample name	solid density g cm ⁻³	BET Surface m ² g ⁻¹	Fe g (100g) ⁻¹	Mn g (100g) ⁻¹	Co mg kg ⁻¹	Pb mg kg ⁻¹
Surface horizon	2.43	nd	3	0.09	13	30
3-4 mm nodules	2.86 ± 0.00	66 ± 4	22 ± 1	1.45 ± 0.18	144 ± 15	59 ± 2
4-5 mm nodules	2.80 ± 0.03	60 ± 4	18 ± 1	2.02 ± 0.15	175 ± 34	48 ± 4
Quartz sand	2.56	0.57 ± 0.09	<DL	<DL	0.54	19.41

[†] When available, arithmetic mean values ± standard deviations were provided; nd = no data; DL = detection limit

Table 2: Main characteristics of the different columns

Treatment	Columns	3-4mm	4-5mm	Quartz	Solid	Pore	Fe	Mn	Co	Pb
		nodule	nodule							
		mass	mass	g	g cm ⁻³	of the				
		g	g			column				
						cm ³				
Saturated	Quartz			96.89	2.56	24	0	0	0.05	1.9
	Nodules 1	34.27	43.53		2.83	34	15	1.4	12	4.1
	Nodules 2	34.2	43.48		2.83	34	15	1.4	12	4.1
14-day cycles	Quartz			97.145	2.56	24	0	0	0.05	1.9
	Nodule	34.24	43.51		2.83	34	15	1.4	12	4.1

Table 3: Equilibrium reactions and associated solubility constants at 25°C and 1 bar, used to construct the Eh-pH diagrams for the different minerals found in the nodules

Minerals	Reactions	log K	References
γ goethite	$\gamma\text{FeOOH} + 3\text{H}^+ + \text{e}^- \leftrightarrow \text{Fe}^{2+} + 2\text{H}_2\text{O}$	16.65	Hashimoto et Misawa (1973)
α goethite	$\alpha\text{FeOOH} + 3\text{H}^+ + \text{e}^- \leftrightarrow \text{Fe}^{2+} + 2\text{H}_2\text{O}$	14.97	Détournay et al. (1975)
green rust	$\text{Fe}(\text{OH})_3 + 3\text{H}^+ + \text{e}^- \leftrightarrow \text{Fe}^{2+} + 3\text{H}_2\text{O}$	15.87	Trolard et Bourrié (1999)
green rust	$\text{Fe}_3(\text{OH})_8 + 8\text{H}^+ + 2\text{e}^- \leftrightarrow 3\text{Fe}^{2+} + 8\text{H}_2\text{O}$	46.41	Ponnamperuma et al. (1967)
ferrihydrite	$\text{Fe}_2\text{O}_3(0.5\text{H}_2\text{O}) + 6\text{H}^+ + 2\text{e}^- \leftrightarrow 2\text{Fe}^{2+} + 3.5\text{H}_2\text{O}$	34.778	Rabenhorst et Castenson (2005)
birnessite	$\text{Mn}_5^{4+}\text{Mn}_2^{3+}\text{O}_{13} + 26\text{H}^+ + 12\text{e}^- \leftrightarrow 7\text{Mn}^{2+} + 13\text{H}_2\text{O}$	249.84 to 258.6	after Parc et al. (1989)
lithiophorite	$\text{Al}_2\text{Mn}_3^{4+}\text{O}_9 + 18\text{H}^+ + 6\text{e}^- \leftrightarrow 2\text{Al}^{3+} + 3\text{Mn}^{2+} + 9\text{H}_2\text{O}$	140.13	after Parc et al. (1989)

Table 4: Average values for the pH and Eh values and Fe, Mn, Co and Pb concentrations according to the water type considered and Fisher's pairwise mean comparison results (ANOVA)

			pH	Eh	Fe	Mn	Co	Pb
Inflow			6.75 ^b	97 ^b	0.33 ^a	0.21 ^c	0.242 ^{cd}	0.006 ^{bc}
Outflow	Continuously saturated	Quartz	7.05 ^a	102 ^b	0.18 ^b	0.24 ^{bc}	0.275 ^{cd}	0.005 ^c
		Nodule 1	7.12 ^a	128 ^a	0.11 ^{cd}	0.25 ^b	0.592 ^b	0.005 ^c
		Nodule 2	7.07 ^a	130 ^a	0.11 ^{cd}	0.31 ^a	0.742 ^a	0.005 ^c
	14-day cycles	Quartz before drying	7.08 ^a	101 ^b	0.17 ^{bc}	0.25 ^b	0.318 ^c	0.008 ^{ab}
		Quartz after drying	7.16 ^a	133 ^a	0.07 ^d	0.11 ^d	0.146 ^d	0.006 ^{bc}
		Nodule before drying	7.05 ^a	147 ^a	0.08 ^d	0.27 ^{ab}	0.589 ^b	0.007 ^{abc}
		Nodule after drying	7.26 ^a	149 ^a	0.05 ^d	0.25 ^{bc}	0.731 ^{ab}	0.010 ^a

a, b, c, d are indicating whether the average are significantly different or not among the different samples with a confident level of 5%

Table 5: Average fraction fixed/released from the different columns for Fe, Mn and Co and Fisher's pairwise mean comparison results (ANOVA)

		Fixed Fe fraction	Released Mn fraction	Released Co fraction
Continuously saturated	Quartz	0.522 ^c	0.139 ^{bc}	0.126 ^c
	Nodule 1	0.660 ^b	0.301 ^{bc}	1.630 ^b
	Nodule 2	0.647 ^b	0.581 ^a	2.383 ^a
14-day cycles	Quartz before drying	0.440 ^c	0.158 ^{bc}	0.182 ^c
	Quartz after drying	0.800 ^{ab}	-0.186 ^c	-0.012 ^c
	Nodule before drying	0.760 ^{ab}	0.394 ^{ab}	1.417 ^b
	Nodule after drying	0.885 ^a	0.373 ^{abc}	2.864 ^a

a, b, c, d are indicating whether the average are significantly different or not among the different samples with a confident level of 5%

Table 6: Amount of leachate collected from the different columns

Treatment	Column	Percolated volume (mL)	Percolated volume (pore volumes)	Percolated volume during the cycle (mL)
Saturated	Quartz	5704	238	987
	Nodule 1	6183	182	1440
	Nodule 2	6565	187	1411
14-day cycles	Quartz	3970	165	0
	Nodule	4225	124	0

Table 7: Total Fe, Mn, Co and Pb gained or lost from the different columns at the end of the experiment, calculated from mass balance calculation on the inflow and outflow waters.

Treatment type	Column type	Fe mg	Mn mg	Co µg	Pb µg
Continuously saturated	Quartz	31	- 8.4	8.3	1
	Nodule 1	69	-11	-102	3.7
	Nodule 2	61	-28	-169	1.4
14-day cycles	Quartz before drying	15	-6.7	-8.8	0.003
	Quartz at the end of the experiment	25	-5.5	-8.6	0.04
	Nodule before drying	27	-11	-57	0.4
	Nodule at the end of the experiment	44	-15	-85	-1.9

Figure caption

Figure 1: Schematic diagram of the experimental design. Qz refers to the quartz columns and C to the nodule ones.

Figure 2: Characteristics of the solution percolating through the topsoil monolith as a function of time: A- pH; B- Eh; C- Fe; D- Mn; E- Co; F- Pb. Dark triangles represent the outflow, while open circles are for the inflow.

Figure 3: Eh-pH stability diagrams for Fe, considering 2 forms of goethite, 2 green rusts and ferrihydrite as Fe oxides, a) for a total Fe concentration in water at 10^{-4} mol L⁻¹ and b) for a total Fe concentration in water at 10^{-5} mol L⁻¹.

Figure 4: Eh-pH stability diagram for Mn, considering total Mn concentration in water = 10^{-4} mol L⁻¹ and birnessite and lithiophorite as Mn oxides. For lithiophorite, a concentration of Al in solution of 10^{-6} mol L⁻¹ was considered. For birnessite a range of stability constant was encountered in the literature (Table 3). The extreme values were used to calculate the stability lines for birnessite and represented as a shaded domain on the figure.

Figure 5: pH, Eh, Fe, Mn, Co and Pb concentrations as a function of the pore volume of the inflow and outflow for the quartz column undergoing permanent saturation. Dark triangles represent the outflow, while open circles are for the inflow.

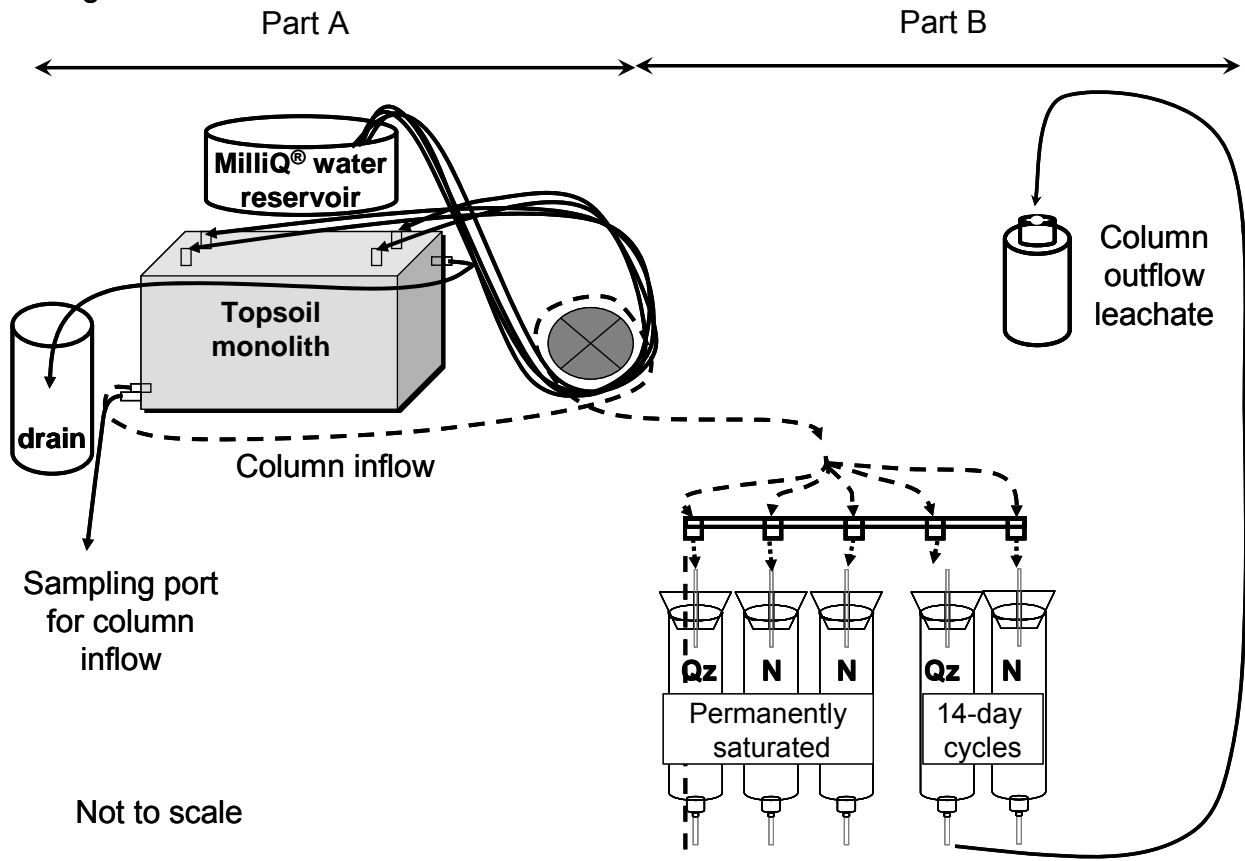
Figure 6: pH, Eh, Fe, Mn, Co and Pb concentrations as a function of the pore volume of the inflow and outflow for nodule columns 1 & 2 undergoing permanent saturation. Dark triangles represent the outflow, while open circles are for the inflow. Black symbols are for the first column, while grey ones state for the second column.

Figure 7: pH, Eh, Fe, Mn, Co and Pb concentrations as a function of the pore volume of the inflow and outflow for the quartz column undergoing 14-day cycles. Dark triangles represent the outflow, while open circles are for the inflow.

Figure 8: pH, Eh, Fe, Mn, Co and Pb concentrations as a function of the pore volume of the inflow and outflow for the nodule column undergoing 14-day cycles. Dark triangles represent the outflow, while open circles are for the inflow.

Figure 9: Iron fixation ratios versus mean Eh values for the different columns.

Fig. 1



insu-00433531, version 1 - 31 Jan 2011

Fig. 2

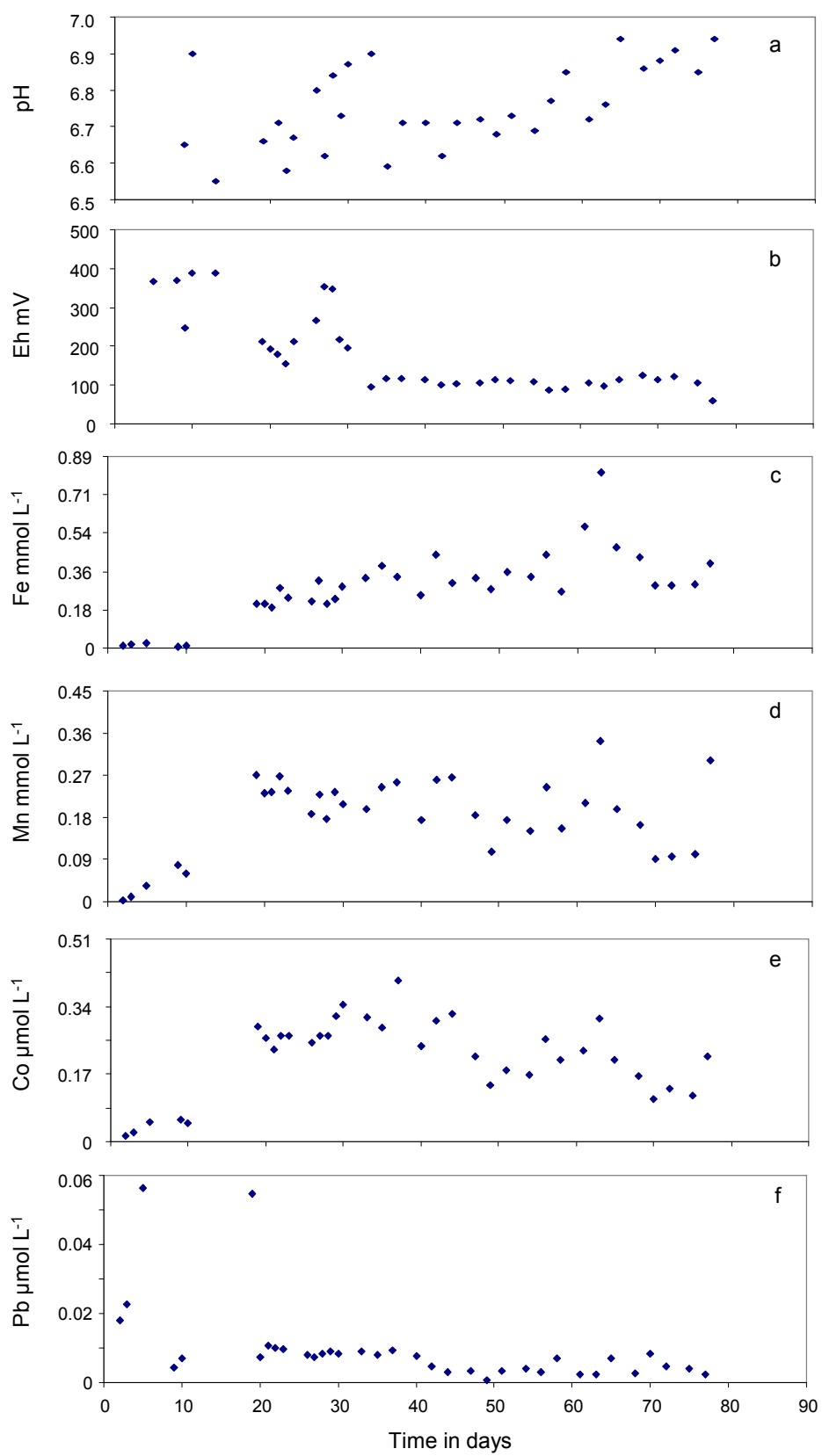


Fig. 3

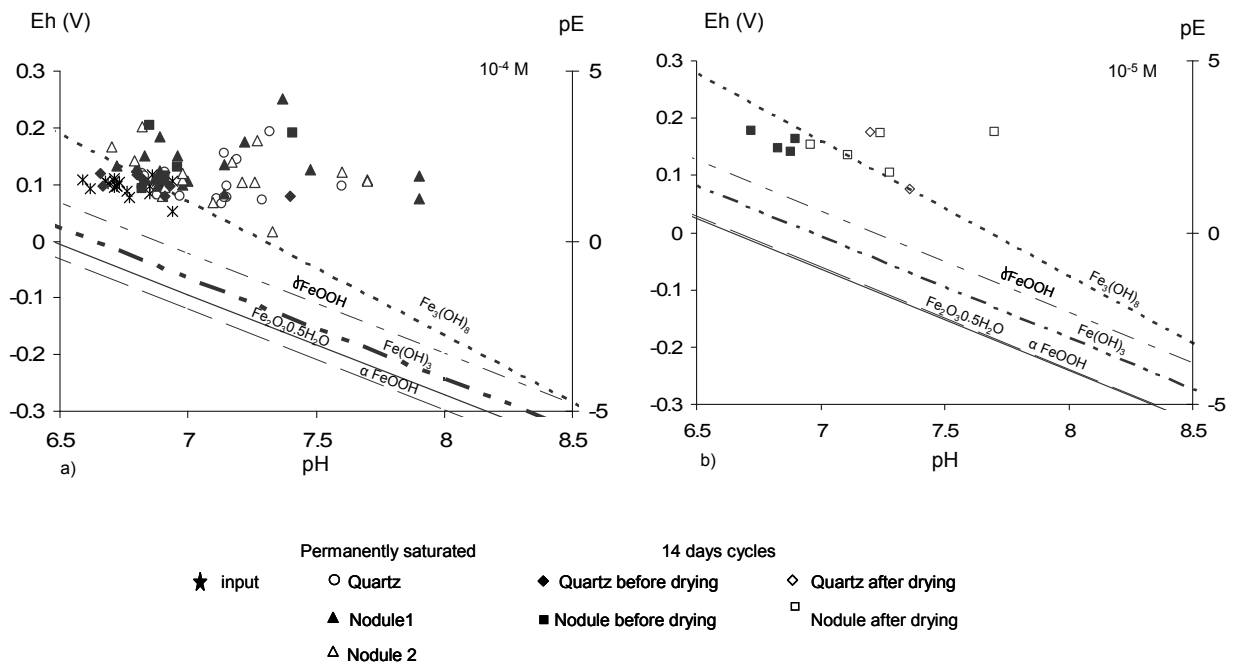


Fig. 4

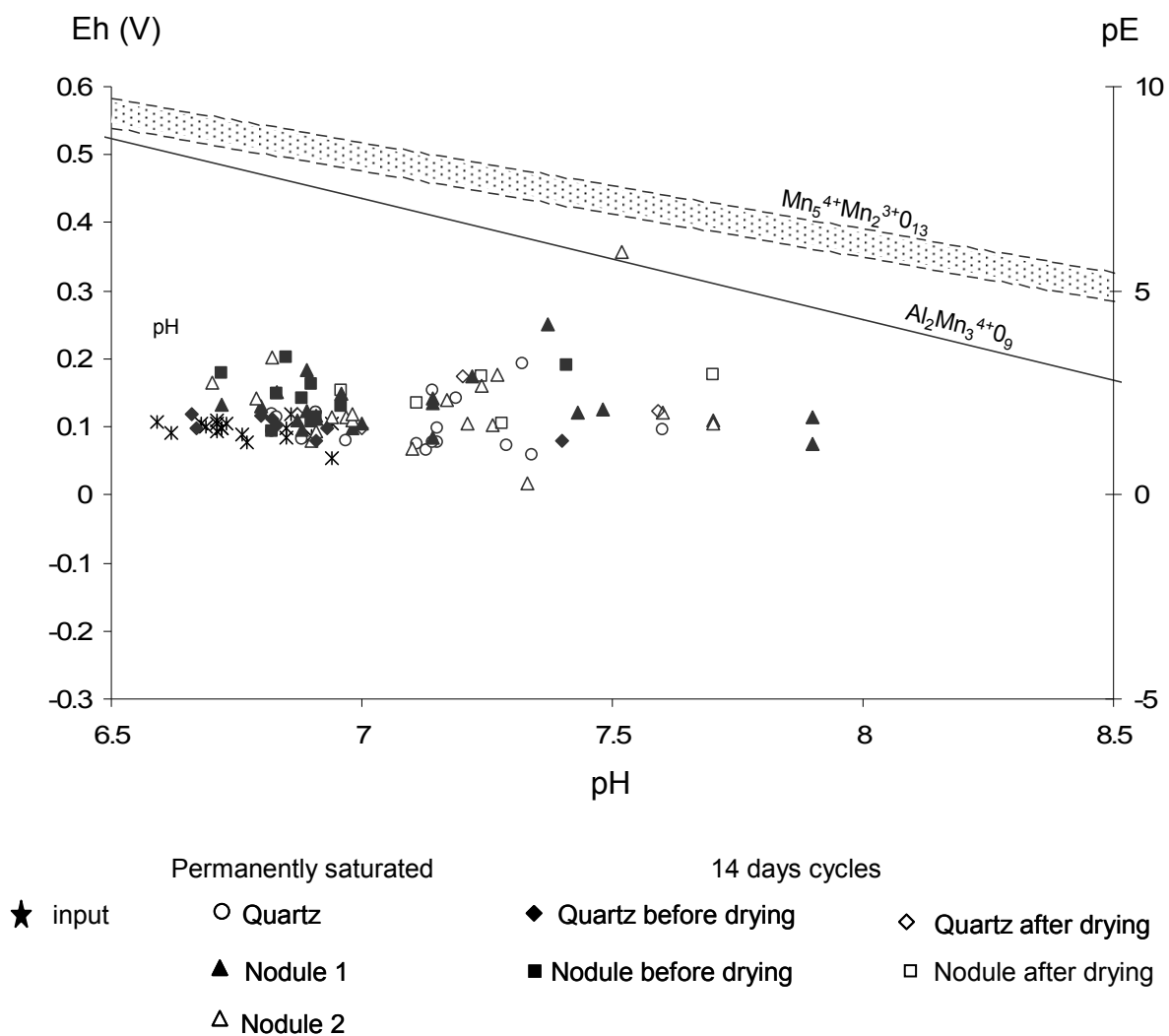


Fig. 5

Quartz column : permanently saturated

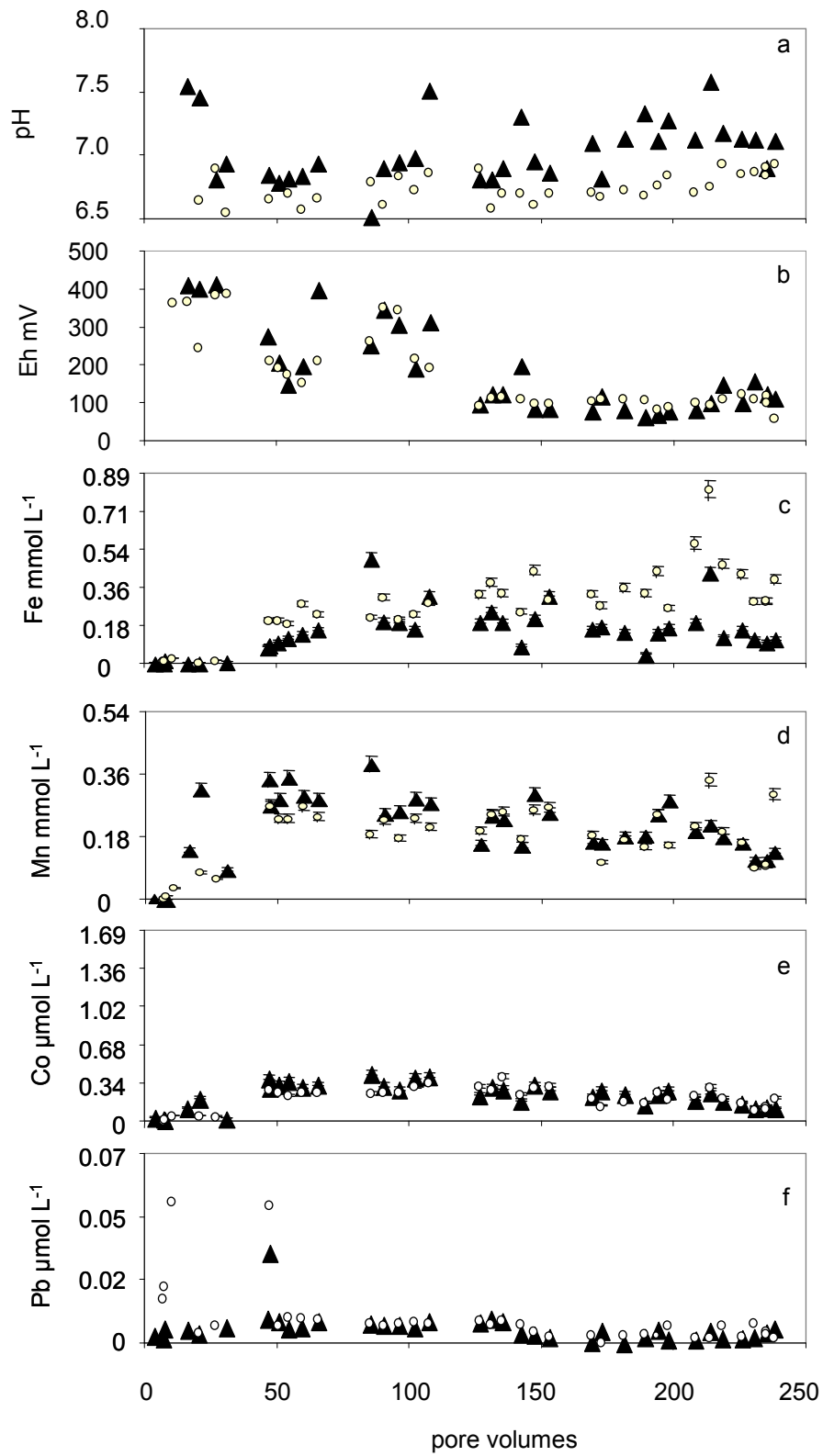
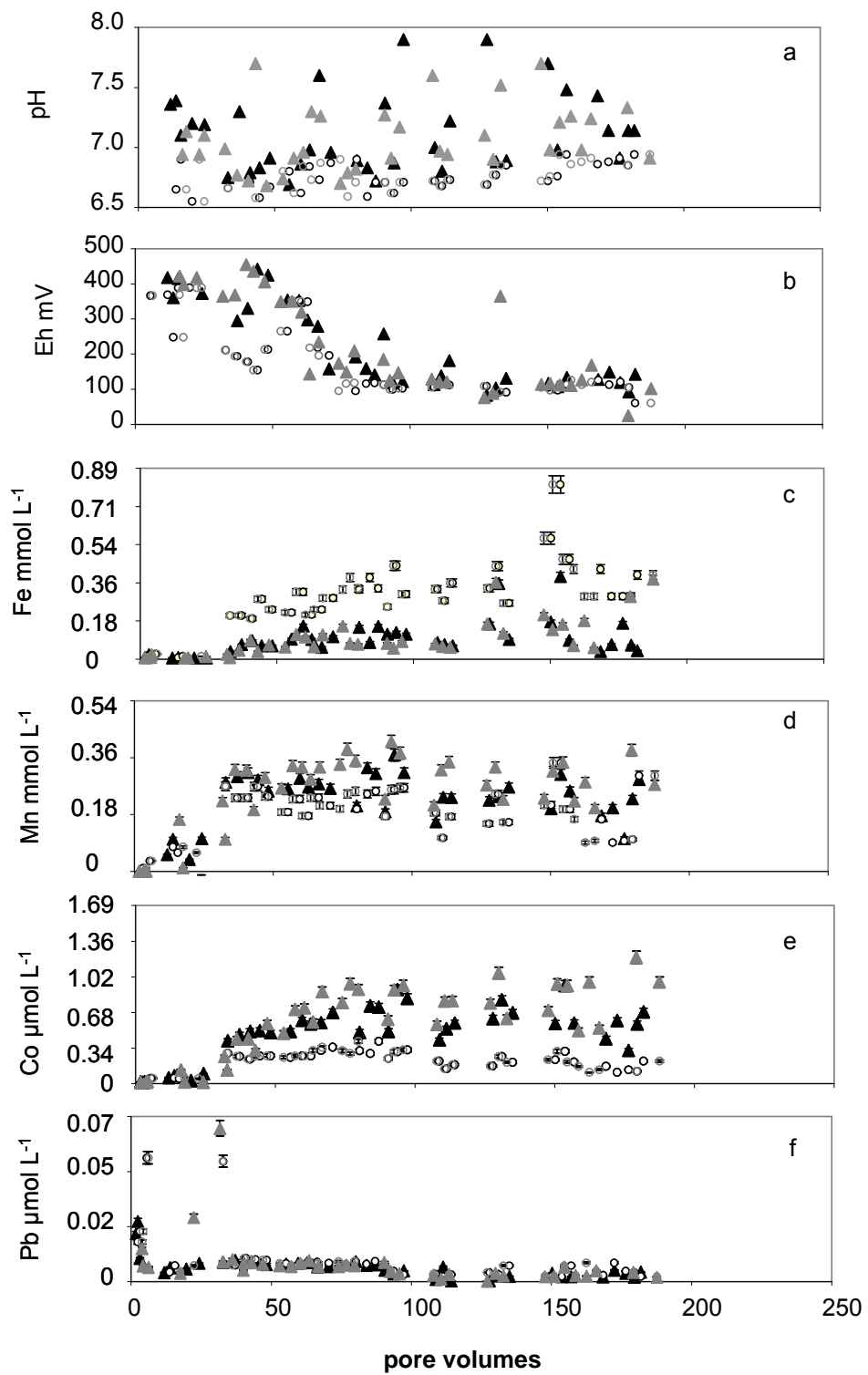


Fig.6

Nodule columns 1 & 2 : permanently saturated



insu-00433531, version 1 - 31 Jan 2011

Fig. 7

Quartz column : 14 day-cycles

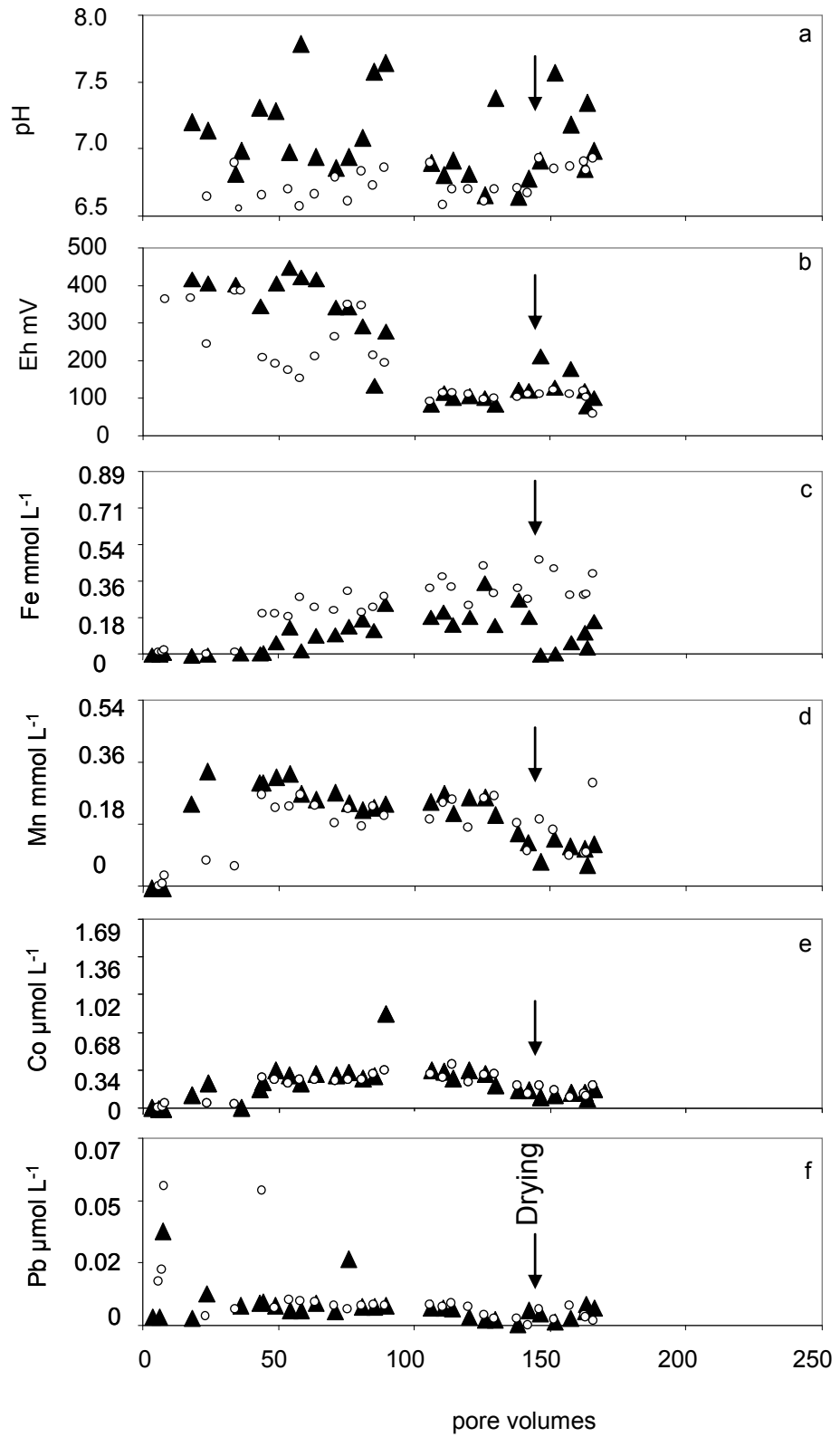


Fig. 8

Nodule column: 14 day-cycles

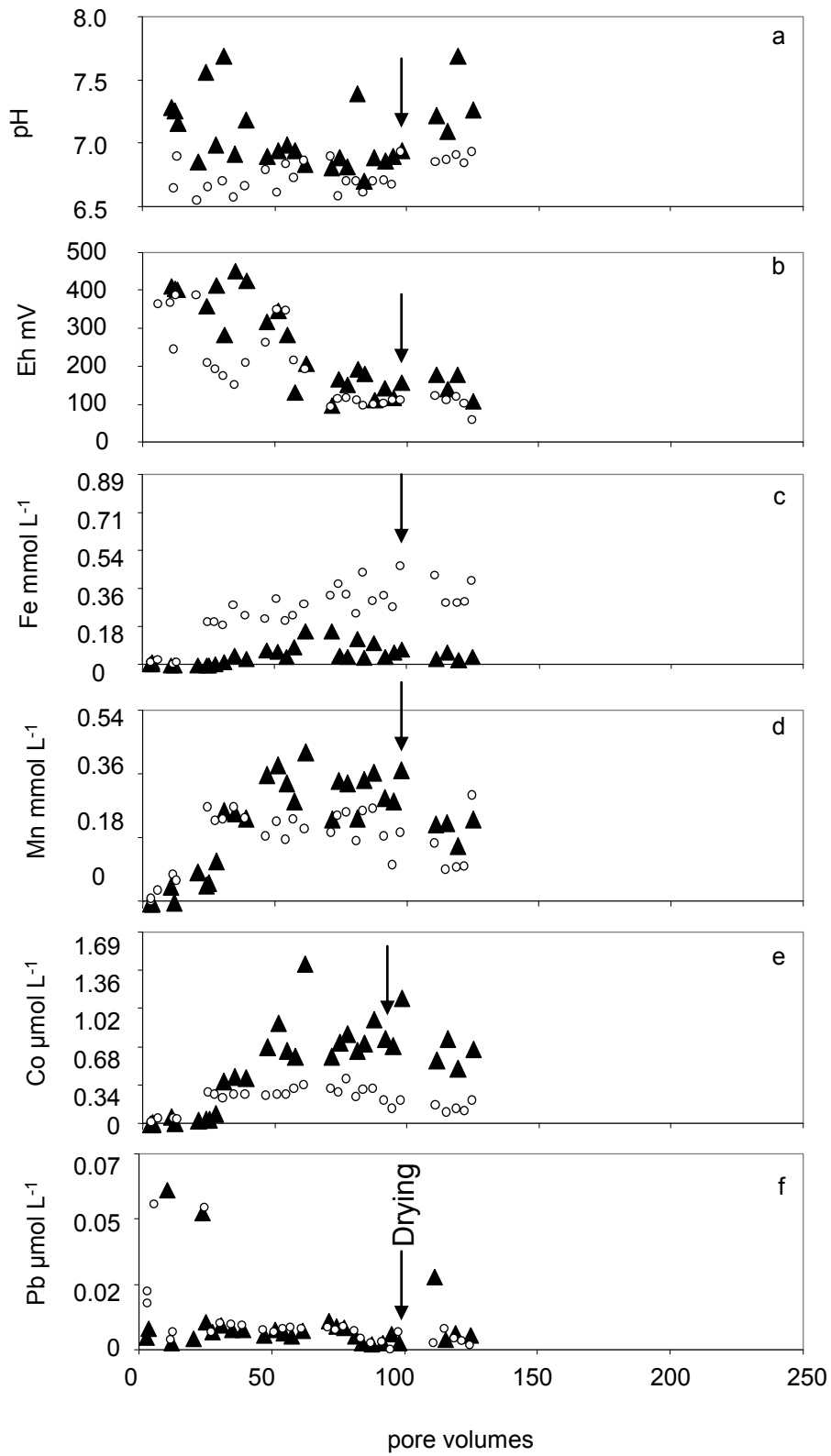


Fig. 9

